Robotica: (2020) volume 38, pp. 1434–1449. © Cambridge University Press 2019
doi:10.1017/S0263574719001553

SLIP-Based Control of Bipedal Walking Based on Two-Level Control Strategy

Behnam Dadashzadeh†* and C.J.B. Macnab‡

†*Faculty of Electrical and Computer Engineering, Mechatronics Engineering Department, University of Tabriz, Tabriz, Iran*
‡*Department of Electrical and Computer Engineering, University of Calgary, Calgary, Canada*
E-mail: cmacnab@ucalgary.ca

(Accepted October 12, 2019. First published online: November 4, 2019)

SUMMARY
In this research, we propose a two-level control strategy for simultaneous gait generation and stable control of planar walking of the Assume The Robot Is A Sphere (ATRIAS) biped robot with unlocked torso, utilizing active spring-loaded inverted pendulum (ASLIP) as reference models. The upper level consists of an energy-regulating control calculated using the ASLIP model, producing reference ground reaction forces (GRFs) for the desired gait. In the lower level controller, PID force controllers for the motors ensure tracking of the reference GRFs for ATRIAS direct dynamics. Meanwhile, ATRIAS torso angle is controlled stably to make it able to follow a point mass template model. Advantages of the proposed control strategy include simplicity and efficiency. Simulation results using ATRIAS's complete dynamic model show that the proposed two-level controller can reject initial condition disturbances while generating stable and steady walking motion.

KEYWORDS: Bipedal walking; Underactuated robot; Two-level control; Force control.

1. Introduction

Using underactuated biped models with point feet to generate walking and running gaits can result in improvements over flat-foot models, both qualitative (more natural looking) and quantitative (greater efficiency). Although standard methods like zero moment point (ZMP)[1] can generate walking and running in fully actuated flat-foot biped robots, underactuated-robot gait generation and control remain active areas of research. One approach utilizes the Poincare return map of the gait stability analysis, applied to passive gaits in ref. [2] and active gaits in ref. [3]. Utilizing the hybrid zero dynamics (HZD) with Poincare map techniques can generate asymptotically stable bipedal walking[4] and running.[5] An event-based discrete LQR controller can stabilize the fixed point in a Poincare map of a passive biped running gait, where the model has springy, massless feet.[6] Previously, the first author extended the previous LQR method to stabilize active fixed points of the Poincare map in more general active gaits.[7]

Another control strategy for underactuated biped robots uses the spring loaded inverted pendulum (SLIP) model proposed by Blickhan.[8] The SLIP-based control approach can generate the same center of mass (COM) trajectory and ground reaction force (GRF) profile as human bipedal walking and running, qualitatively speaking.[9] For a restricted range of initial condition inside a basin of attraction, the SLIP model shows stable walking and running gaits, but outside this region SLIP has periodic unstable gaits. Thus, researchers have proposed several active SLIP, or ASLIP, architectures and controllers, for example, an energy-level control in stance phase,[10] swing leg retraction,[11] dead-beat control,[12] and variable free-leg length and stiffness.[13]

Due to the SLIP model's advantages (including stability and energy efficiency), using it as a simple reference model in order to produce walking and running biped gaits for more complicated machines

* Corresponding author. E-mail: b.dadashzadeh@tabrizu.ac.ir

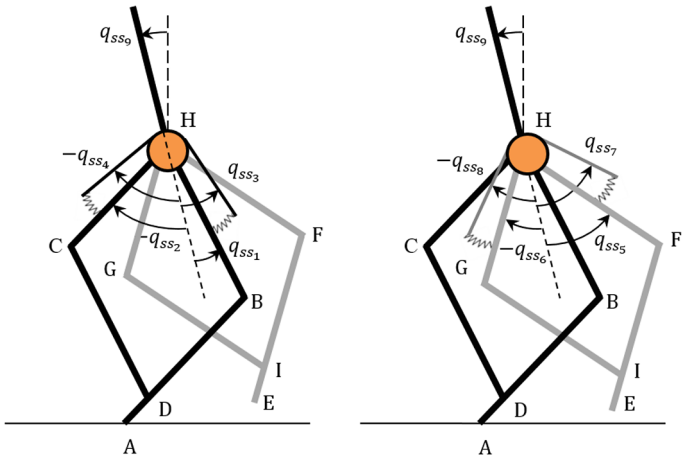

Fig. 1. Generalized coordinates of ATRIAS in single-support phase.

is a possible approach – one pursued in this paper. The challenge in this approach is due to multibody robots differing significantly from the SLIP model: more degrees of freedom, additional torso angle control, and significant energy losses and discontinuities in touchdown. A three-link hopper tracked a SLIP trajectory, using feedback linearization in ref. [14] and HZD in ref. [15]. Garoffalo[16] presented a two-level control strategy for walking in a five-link rigid biped model by following a SLIP trajectory; they used feedback linearization in the lower level controller, but we use their idea for a higher level energy-regulating control in this paper.

In previous work, the first author proposed a two-level controller for generating running gaits for the 'Assume The Robot Is A Sphere' (ATRIAS) robot at Oregon State University,[17] with an active SLIP stabilization and ATRIAS leg-force control occurring in each running phase. SLIP model was used for dimension reduction of ATRIAS planar[18] and 3D[19] walking model by using HZD method. Rezazadeh[20] proposed a step-by-step control strategy for ATRIAS walking, including foot placement, leg length adjustment, and torso stabilization. In some recent works, Gupta et al.[21] optimized walking gait variables and utilized artificial neural networks for generating walking gaits on uneven surfaces. Janardhan et al.[22] investigated biped trajectory generation for crossing large ditches and proposed point of feasibility to bring the robot to rest at the end of ditch crossing. Kajita et al.[23] controlled HRP-2Kai walking by discretizing the continuous system by a constant unit length along the walking direction. Our work differs from these works by utilizing a basic template model to generate gait.

In this work, we present a two-level controller for SLIP-based stable walking of multibody biped robots with legs and torso inertia. In the upper level control, active SLIP models provide simple reference models for each phase – controlled so as to return to the nominal SLIP trajectory. The resulting GRFs from the trajectory become reference signals in the lower level control. The lower level control regulates the leg force of the stance leg and the trajectory of the swing leg in ATRIAS. In this way, the higher level control provides the motor controllers with reasonable tracking error, that is, avoiding actuator saturation. We view this as a generalization of the two-level running controller[17] to walking. Our method significantly differs from previous works[15, 16, 18–20] by using force control in the stance leg to track stabilized SLIP gaits, motivated by the fact that force control provides particular advantages for walking and running on soft terrain.[24] We demonstrate the beneficial effect of swing leg trajectory planning on overall gait stability through simulations using a full dynamic simulation of ATRIAS.[24]

2. Dynamic Modeling of ATRIAS Walking

A walking gait includes a single-support phase, a touchdown event, a double-support phase, and a takeoff event. In this paper, we consider planar walking of ATRIAS on the sagittal plane. Each leg of ATRIAS contains a four-bar mechanism, as well as two motors in the hip which actuate the upper links (Fig. 1). The robot legs in the sagittal plane contain four brushless motors with torques u_1, u_2, u_3, and u_4: exerted between torso and links BH, CH, FH, and GH, respectively. A bending

https://doi.org/10.1017/S0263574719001553 Published online by Cambridge University Press

Table I. Kinematic and kinetic parameters of ATRIAS dynamic model.

Quantity	Value (in SI units)	Description
$m_1, l_1, a_1, \bar{I}_1$	0.626, 0.5, 0.1691, 0.0198	Mass, length, COM, and moment of inertia of the links BH and FH
$m_2, l_2, a_2, \bar{I}_2$	0.609, 0.4, 0.1462, 0.0156	Mass, length, COM, and moment of inertia of the links CH and GH
$m_3, l_3, a_3, \bar{I}_3$	0.510, 0.5, 0.1055, 0.0143	Mass, length, COM, and moment of inertia of the links AB and EF
$m_4, l_4, a_4, \bar{I}_4$	0.475, 0.5, 0.0788, 0.0109	Mass, length, COM, and moment of inertia of the links CD and GI
$m_s, a_{s1}, a_{s2}, \bar{I}_s$	1.704, 0.0448, 0.0726, 0.0231	Mass, COM position, and moment of inertia of the spring complex
$m_9, a_9, \bar{I}_9$	50.647, 0.1873, 3.8316	Mass, COM, and moment of inertia of the torso
K_g	50	Gear reduction ratio of the harmonic drive
$\bar{K}$	0.0987	Torque constant of the motors (N m/A)
J_r	0.00121	Moment of inertia of rotor and harmonic drive (kg.m^2)
K_s	4119	Torsional spring stiffness (N m/rad)
C_s	1.46	Damping ratio of spring (N m s/rad)
C_{hd}	19.0	Damping ratio of harmonic drive (N m s/rad)

plate between each motor shaft and its corresponding leg link acts as a torsional spring in series to each motor. Also, a harmonic drive with a reduction ratio of 50:1 provides sufficient torque. The robot has point feet (no actuators), making the system underactuated. A boom, connected to the torso, constrains the robot to move in a circular path on the sagittal plane. We assume the torso angle on the sagittal plane should be controlled by the leg motors. The calculations of the torso mass and moment of inertia include all the components with motors mounted. We model the damping of the springs and the harmonic drives as linear and velocity-dependent. ATRIAS kinematic, mass, and damping parameters are shown in Table I.

2.1. Single-support phase

In the single-support phase, leg 1 provides the support (Fig. 1). It has a passive revolute joint and touches the ground at point A. Leg 2 swings around the hip. Each leg has 4 degrees of freedom (DOF), including two independent angles for the leg links (connected to the output side of the springs) and two independent angles for the harmonic-drive output shafts (connected to the input side of the springs). Thus, the robot has 9 DOF in single-support phase, and we designate the generalized coordinates by $\left[\mathbf{q}_{ss}\right]_{9\times1}$. Using Lagrange's equation with dissipations is

$$\frac{d}{dt}\left(\frac{\partial L}{\partial \dot{\mathbf{q}}}\right) - \frac{\partial L}{\partial \mathbf{q}} + \frac{\partial R}{\partial \dot{\mathbf{q}}} = \mathbf{Q} \tag{1}$$

where L is the Lagrangian function, $\mathbf{Q}$ is the generalized coordinates vector, and Raileigh dissipation function R includes damping power of the harmonic drives and springs. The result is the ATRIAS single-support dynamic model

$$\left[\mathbf{D}_{ss}\left(\mathbf{q}_{ss}\right)\right]_{9\times9} \cdot \left[\ddot{\mathbf{q}}_{ss}\right]_{9\times1} + \left[\mathbf{C}_{ss}\left(\mathbf{q}_{ss}, \dot{\mathbf{q}}_{ss}\right)\right]_{9\times1} = \left[\mathbf{B}_{ss}\right]_{9\times4} \cdot \left[\mathbf{u}\right]_{4\times1} \tag{2}$$

where $\mathbf{D}_{ss}$ is the inertia matrix, $\mathbf{C}_{ss}$ contains Coriolis and gravity terms, and $\mathbf{B}_{ss}$ is the input matrix. Because motor torques are exerted to the inputs of harmonic drives of links 3, 4, 7, and 8, the input matrix is

$$\mathbf{B}_{ss} = K_g \begin{bmatrix} 0 & 0 & 1 & 0 & 0 & 0 & 0 & 0 & 0 \\ 0 & 0 & 0 & 1 & 0 & 0 & 0 & 0 & 0 \\ 0 & 0 & 0 & 0 & 0 & 0 & 1 & 0 & 0 \\ 0 & 0 & 0 & 0 & 0 & 0 & 0 & 1 & 0 \end{bmatrix}^T \tag{3}$$

https://doi.org/10.1017/S0263574719001553 Published online by Cambridge University Press

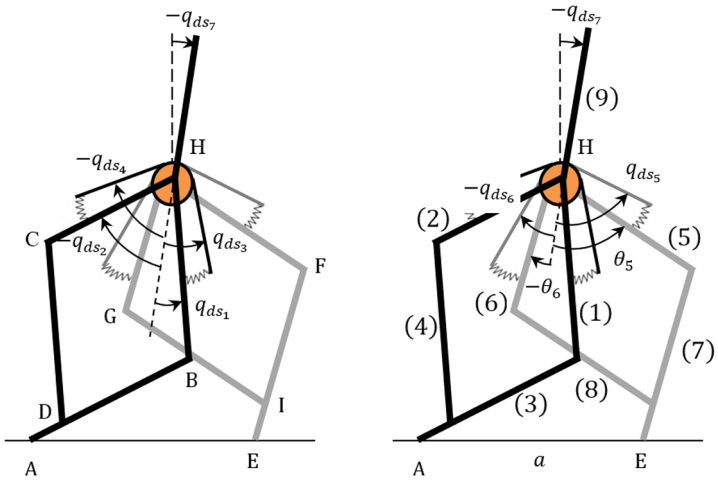

Fig. 2. Generalized coordinates and numbers of the links of ATRIAS in double-support phase.

2.2. *Touchdown event*

The touchdown event occurs at the end of the single-support phase, when contact point E touches the ground. So, an impact $\widehat{\boldsymbol{F}} = \hat{F}_x \boldsymbol{i} + \hat{F}_y \boldsymbol{j}$ affects point E in the stance dynamic model. Lagrange's impact model for this event becomes

$$D_{ss}\left(q_{ss}\right) . \left(\dot{q}_{ss}^{+} - \dot{q}_{ss}^{-}\right) = \hat{Q} \tag{4}$$

in which superscripts + and − show instances just after and before touchdown, and generalized impact $\widehat{\mathbf{Q}}$ is written as a function of $\hat{F}_x$ and $\hat{F}_y$ using virtual work. Also, the relationship between single-support and double-support generalized coordinates provides two more equations for finding the unknowns.

$$\begin{bmatrix} \dot{q}_{ss_5}^{+} \\ \dot{q}_{ss_6}^{+} \end{bmatrix} = \begin{bmatrix} \dot{\theta}_5\left(q_{ds}^{+}, \dot{q}_{ds}^{+}\right) - \dot{q}_{ds_7}^{+} \\ \dot{\theta}_6\left(q_{ds}^{+}, \dot{q}_{ds}^{+}\right) - \dot{q}_{ds_7}^{+} \end{bmatrix} \tag{5}$$

Double-support phase generalized coordinates and angles θ_5 and θ_6 appear in Fig. 2(b). Equations (4) and (5) constitute a touchdown map whose solution provides an initial condition for the double-support phase.

2.3. *Double-support phase*

In the double-support phase, both feet are pivoted to the ground with a known distance a (Fig. 2). Angles θ_5 and θ_6 are dependent variables, and we derive 7 DOF equations of motion of this phase instead of solving 9 DOF equations (2) with two holonomic constraint equations. Leg 1 is the rear leg and leg 2 is the front leg. The equations of motion in double-support phase in terms of the double-support generalized coordinates $\mathbf{q}_{ds}$ become

$$\left[\mathbf{D}_{ds}\left(\mathbf{q}_{ds}\right)\right]_{7\times 7} . \left[\ddot{\mathbf{q}}_{ds}\right]_{7\times 1} + \left[\mathbf{C}_{ds}\left(\mathbf{q}_{ds}, \dot{\mathbf{q}}_{ds}\right)\right]_{7\times 1} = \left[\mathbf{B}_{ds}\right]_{7\times 4} . \left[\mathbf{u}\right]_{4\times 1} \tag{6}$$

where the input matrix is defined as

$$B_{ds} = K_g \begin{bmatrix} 0 & 0 & 1 & 0 & 0 & 0 & 0 \\ 0 & 0 & 0 & 1 & 0 & 0 & 0 \\ 0 & 0 & 0 & 0 & 1 & 0 & 0 \\ 0 & 0 & 0 & 0 & 0 & 1 & 0 \end{bmatrix}^T \tag{7}$$

2.4. *Takeoff event*

The takeoff event occurs at the precise moment in the double-support phase when the vertical GRF of leg 1 becomes zero, while the vertical GRF of leg 2 is positive. In simulations, the takeoff event can be detected by mapping motor torques to GRF components and finding the root of $GRF_{y,1}$.

https://doi.org/10.1017/S0263574719001553 Published online by Cambridge University Press

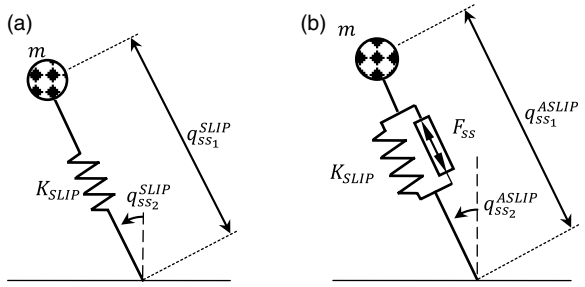

Fig. 3. Generalized coordinates of (a) SLIP and (b) ASLIP models in single-support phase.

By neglecting the masses of the leg links compared with the torso mass, the torque-force map as a function of double-support coordinates becomes

$$\begin{bmatrix} GRF_{x,i} \\ GRF_{y,i} \end{bmatrix} = - \begin{bmatrix} l_1 \cos(q_1 + q_7) & l_1 \sin(q_1 + q_7) \\ l_3 \cos(-q_2 - q_7) & l_3 \sin(-q_2 - q_7) \end{bmatrix}^{-1} \begin{bmatrix} T_i^s \\ T_{i+1}^s \end{bmatrix} \tag{8}$$

in which $GRF_{x,i}$ and $GRF_{y,i}$ are components of the GRF on leg i, and T_i^s and T_{i+1}^s are spring torques of leg i in the counterclockwise direction.

The takeoff is an energy-conserved event without any impact discontinuities or velocity discontinuities; thus, its map is defined by converting the link labels between the two phases as (9) in which superscripts + and − show instances just after and before takeoff.

$$\mathbf{q}_{ss}^{+} = \left[\theta_5\left(\mathbf{q}_{ds}^{-}\right), \theta_6\left(\mathbf{q}_{ds}^{-}\right), q_{ds_5}^{-}, q_{ds_6}^{-}, q_{ds_1}^{-}, q_{ds_2}^{-}, q_{ds_3}^{-}, q_{ds_4}^{-}, q_{ds_7}^{-}\right]^T \tag{9}$$

2.5. Hybrid model of walking

The walking hybrid model includes both single-support and double-support continuous-time equations and instantaneous-events maps. In this map, $\mathbf{x}_{ss} = \left[\mathbf{q}_{ss}; \dot{\mathbf{q}}_{ss}\right]$ denotes the state vector of the single-support phase and $\mathbf{x}_{ds} = \left[\mathbf{q}_{ds}; \dot{\mathbf{q}}_{ds}\right]$ for the double-support phase. The Poincare section S_1 consists of the set of $\mathbf{x}_{ss}$ vectors that reaches the touchdown event, and the set of $\mathbf{x}_{ds}$ vectors that reaches the takeoff event defines set S_2.

$$\begin{cases} \dot{\mathbf{x}}_{ss} = \mathbf{f}_{ss}(\mathbf{x}_{ss}) + \mathbf{g}_{ss}(\mathbf{x}_{ss})\,\mathbf{u}_{ss} \\ \mathbf{x}_{ds}^{+} = \Delta_{ss}^{ds}\left(\mathbf{x}_{ss}^{-}\right), \ \ \mathbf{x}_{ss}^{-} \in S_1 \\ \dot{\mathbf{x}}_{ds} = \mathbf{f}_{ds}(\mathbf{x}_{ds}) + \mathbf{g}_{ds}(\mathbf{x}_{ds})\,\mathbf{u}_{ds} \\ \mathbf{x}_{ss}^{+} = \Delta_{ds}^{ss}\left(\mathbf{x}_{ds}^{-}\right), \ \ \mathbf{x}_{ds}^{-} \in S_2 \end{cases} \tag{10}$$

3. Passive and Active SLIP Walking

Passive and active SLIP models consist of a point mass and massless legs, so their takeoff and touchdown events occur without energy losses or velocity discontinuities. Successive models of single-support phase, touchdown map, double-support phase, and takeoff map constitute the SLIP walking model.

3.1. Single-support phase

In the single-support phase of SLIP, the stance leg consists of a massless linear spring bearing a point mass m pivoted to the ground (Fig. 3). The massless swing leg pivots about the hip and is assumed to clear the ground without extra energy expenditure. The spring stiffness of the leg is K_{SLIP}, and the free leg length is l_0. The single-support generalized coordinates are chosen as $\mathbf{q}_{ss}^{\mathrm{SLIP}}=[l, \theta]^T$ in which l is the stance leg length and θ is the stance leg angle with respect to vertical (Fig. 3(a)). The dynamic model of the single-support phase for passive SLIP is

$$\left[\mathbf{D}_{ss}^{\mathrm{SLIP}}\left(\mathbf{q}_{ss}^{\mathrm{SLIP}}\right)\right]_{2\times 2} \cdot \left[\ddot{\mathbf{q}}_{ss}^{\mathrm{SLIP}}\right]_{2\times 1} + \left[\mathbf{C}_{ss}^{\mathrm{SLIP}}\left(\mathbf{q}_{ss}^{\mathrm{SLIP}}, \dot{\mathbf{q}}_{ss}^{\mathrm{SLIP}}\right)\right]_{2\times 1} = 0 \tag{11}$$

in which $\mathbf{D}_{ss}^{\mathrm{SLIP}}$ and $\mathbf{C}_{ss}^{\mathrm{SLIP}}$ are well-known matrices.[25]

https://doi.org/10.1017/S0263574719001553 Published online by Cambridge University Press

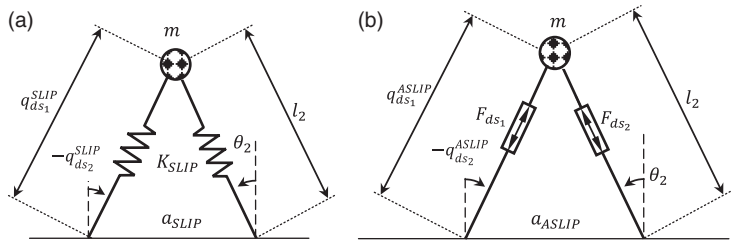

Fig. 4. Generalized coordinates of (a) SLIP and (b) ASLIP models in double-support phase.

An active SLIP (ASLIP) model for the stance phase with a force actuator parallel to the leg spring that will be appropriate for our control strategy is shown in Fig. 3(b). The generalized coordinates of ASLIP $\mathbf{q}_{ss}^{\text{ASLIP}}$ remains the same as in the SLIP model. The dynamic model of the ASLIP in stance phase becomes

$$\left[\mathbf{D}_{ss}^{\text{ASLIP}}\left(\mathbf{q}_{ss}^{\text{ASLIP}}\right)\right]_{2\times 2}\cdot\left[\ddot{\mathbf{q}}_{ss}^{\text{ASLIP}}\right]_{2\times 1}+\left[\mathbf{C}_{ss}^{\text{ASLIP}}\left(\mathbf{q}_{ss}^{\text{ASLIP}},\dot{\mathbf{q}}_{ss}^{\text{ASLIP}}\right)\right]_{2\times 1}=\left[\mathbf{B}_{ss}^{\text{ASLIP}}\right]_{2\times 1}.F_{ss} \tag{12}$$

in which control input F_{ss} is the force of the leg actuator and the coefficient matrices can be obtained easily.

3.2. Double-support phase

In the double-support phase, both legs pivot from the ground with a known distance of a (Fig. 4). The SLIP model in the double-support phase has 2 DOF with generalized coordinates $\mathbf{q}_{\text{ds}}^{\text{SLIP}}$, as shown in Fig. 4(a). Given a known step length a from touchdown configuration, we can write the length and angle of leg 2 as a function of $\mathbf{q}_{ds}^{\text{SLIP}}$. The dynamic model of the SLIP model in double-support phase is

$$\left[\mathbf{D}_{ds}^{\text{SLIP}}\left(\mathbf{q}_{ds}^{\text{SLIP}}\right)\right]_{2\times 2}\cdot\left[\ddot{\mathbf{q}}_{ds}^{\text{SLIP}}\right]_{2\times 1}+\left[\mathbf{C}_{ds}^{\text{SLIP}}\left(\mathbf{q}_{ds}^{\text{SLIP}},\dot{\mathbf{q}}_{ds}^{\text{SLIP}}\right)\right]_{2\times 1}=0 \tag{13}$$

In the double-support phase, our model uses a simple force actuator in series in each leg (Fig. 4(b)); thus, it becomes an active SLIP model, with 2 DOF and full controllability. The proposed model provides a simple efficient model to use in calculating a way to return the system to the desired trajectory. Using the generalized coordinates $\mathbf{q}_{ds}^{\text{ASLIP}}$, its dynamic equation is written as

$$\left[\mathbf{D}_{ds}^{\text{ASLIP}}\left(\mathbf{q}_{ds}^{\text{ASLIP}}\right)\right]_{2\times 2}\cdot\left[\ddot{\mathbf{q}}_{ds}^{\text{ASLIP}}\right]_{2\times 1}+\left[\mathbf{C}_{ds}^{\text{ASLIP}}\left(\mathbf{q}_{ds}^{\text{ASLIP}},\dot{\mathbf{q}}_{ds}^{\text{ASLIP}}\right)\right]_{2\times 1}=\left[\mathbf{B}_{ds}^{\text{ASLIP}}\left(\mathbf{q}_{ds}^{\text{ASLIP}}\right)\right]_{2\times 2}\cdot\left[\mathbf{F}_{ds}\right]_{2\times 1} \tag{14}$$

in which control vector $\mathbf{F}_{ds}=\left[F_{ds_1},F_{ds_2}\right]^T$ contains the forces of leg actuators, positive in the extending direction. Also, using the concept of virtual work produces the input matrix

$$\mathbf{B}_{ds}^{\text{ASLIP}}=\begin{bmatrix}1 & \dfrac{q_{ds_1}^{\text{ASLIP}}+a\sin q_{ds_2}^{\text{ASLIP}}}{\sqrt{\left(q_{ds_1}^{\text{ASLIP}}\right)^2+a^2+2aq_{ds_1}^{\text{ASLIP}}\sin q_{ds_2}^{\text{ASLIP}}}}\\ 0 & \dfrac{aq_{ds_1}^{\text{ASLIP}}\cos q_{ds_2}^{\text{ASLIP}}}{\sqrt{\left(q_{ds_1}^{\text{ASLIP}}\right)^2+a^2+2aq_{ds_1}^{\text{ASLIP}}\sin q_{ds_2}^{\text{ASLIP}}}}\end{bmatrix} \tag{15}$$

4. Controller Design

The controller aims to make the real robot follow the SLIP dynamics (specifically its GRF profile) and generate a stable walking gait. To have SLIP-like dynamics, ATRIAS uses torsional springs in series with the motors (note control methods like feedback linearization[14] are not possible because series-elastic actuation would cause a singularity in the control law[25]). In this research, we use a force control that, given a known initial condition, will result in a leg GRF profile that brings the system back to the desired trajectory.

First, an optimization problem/solution produces a periodic gait with constant forward velocity.

$$\begin{aligned}&\min_{\mathbf{x}_{ss0}^{\text{SLIP}}(k),\,\theta_{TD}} && \left\|\mathbf{x}_{ss0}^{\text{SLIP}}(k+1)-\mathbf{x}_{ss0}^{\text{SLIP}}(k)\right\|\\ &s.t. && V_{x0}=V_{x,d}\end{aligned} \tag{16}$$

https://doi.org/10.1017/S0263574719001553 Published online by Cambridge University Press

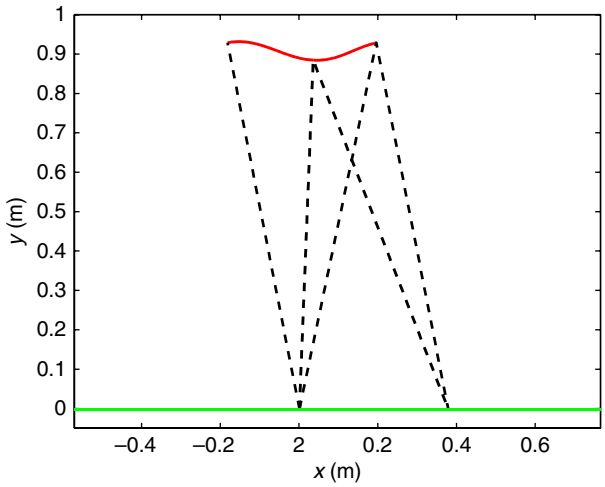

Fig. 5. COM trajectory of SLIP periodic walking with forward velocity of 1.15 m/s.

The cost functional for minimization is defined by the norm of the error of the initial state $\mathbf{x}_{ss0}^{\text{SLIP}} = \left[l_0, \theta_0, \dot{l}_0, \dot{\theta}_0\right]^T$ of the current step to the next step. The constraint is that the initial horizontal velocity V_{x0} has to be equal to the desired forward velocity $V_{x,d}$. The optimization parameters consist of the initial state of the SLIP single-support phase $\mathbf{x}_{ss0}^{\text{SLIP}}$ and the attack angle θ_{TD}. The algorithm performs numerical simulation of the SLIP walking dynamic equations, using these initial conditions, to calculate the trajectory of the periodic SLIP walking gait (COM trajectory shown by solid line in Fig. 5).

We utilize a two-level control strategy to make ATRIAS follow the desired SLIP gait. Because the periodic SLIP gait is unstable, tracking it directly in successive steps will accumulate error and result in an unstable walking motion. To make the system return to the desired path, we propose an intermediate ASLIP model for each phase. Thus, the upper level controller runs in simulation on the reference ASLIP model, bringing the simulated SLIP back to the desired trajectory. The lower level control produces signals for the ATRIAS motors to track the commanded GRF profile resulting from the reference SLIP simulation.

4.1. Upper level controller

In the upper level controller, SLIP is the template and ASLIP is its anchor. ATRIAS has deviations from the desired path at the beginning of each phase and ASLIP has the same initial condition as ATRIAS. We choose an appropriate ASLIP model for each walking phase appropriate for its initial errors, returning it to the desired SLIP trajectory.

4.1.1. Single-support phase. ATRIAS with an unlocked torso has no external torques exerted from the ground to the leg or to the torso, and its only control input is its leg force. Its equivalent ASLIP model should have a similar structure in order to serve as an efficient template for the real robot. Thus, we consider the ASLIP model for this phase as illustrated in Fig. 4(b), with a force actuator parallel to the leg spring. This system is underactuated and classic controllers are not applicable for trajectory tracking. Therefore, we use a SLIP energy-level control law[15] for the model given in (12) as below so that the ASLIP force actuator can return it to the desired (constant) energy level of SLIP

$$F_{ss}(t) = -K_p^E \dot{q}_{ss_1}^{\text{ASLIP}} \left[E(t) - \bar{E}\right] \tag{17}$$

in which K_p^E is a positive proportional coefficient, $q_{ss_1}^{\text{ASLIP}}$ is the stance leg length (Fig. 3(b)), $E(t)$ is the ASLIP mechanical energy, and $\bar{E}$ is the SLIP constant mechanical energy. To understand the intention of the control law, consider that if the leg is contracting and the energy of the system is larger than the nominal energy level, then the controller increases the leg force in order to slow down the mass (and vice versa). If the leg is extracting and the energy of the system is larger than the nominal energy level, then the controller decreases the leg force in order to slow

https://doi.org/10.1017/S0263574719001553 Published online by Cambridge University Press

down the mass (and vice versa). Because the motors of the real robot will not able to track large deviations in the leg force, the ASLIP dynamic equations (12) are solved with control law (17) to return it the nominal gait (Fig. 5). Then the ASLIP trajectory and its toe force profiles are derived numerically.

Note that the swing leg desired angle before touchdown would be

$$\theta_d = \theta_{TD} \tag{18}$$

4.1.2. Double-support phase. The 2 DOF fully actuated ASLIP model in double-support phase (Fig. 4(b)) is controlled using feedback linearization to track the desired SLIP trajectory. The vector of tracking error is defined as the subtraction of ASLIP and SLIP generalized coordinates in the double-support phase

$$\mathbf{e} = \mathbf{q}_{ds}^{\text{ASLIP}} - \mathbf{q}_{ds}^{\text{SLIP}} \tag{19}$$

To achieve $\ddot{\mathbf{e}} + \mathbf{K}_d\,\dot{\mathbf{e}} + \mathbf{K}_p\mathbf{e} = 0$, we derive the ASLIP control law for double-support phase as

$$\mathbf{F}_{ds} = \left(\mathbf{B}_{ds}^{\text{ASLIP}}\right)^{-1}\left(\mathbf{C}_{ds}^{\text{ASLIP}} - D_{ds}^{\text{ASLIP}}\left(\mathbf{D}_{ds}^{\text{SLIP}}\right)^{-1}\mathbf{C}_{ds}^{\text{SLIP}} - \mathbf{D}_{ds}^{\text{ASLIP}}\mathbf{K}_d\dot{\mathbf{e}} - \mathbf{D}_{ds}^{\text{ASLIP}}\mathbf{K}_p\mathbf{e}\right) \tag{20}$$

where $\mathbf{K}_p$ and $\mathbf{K}_d$ are 2×2 matrices that can be appropriately selected to have asymptotically stable response with a desired overshoot and rise time. The values of these controller coefficients have a critical effect on the overall stability of the robot walking. We select these matrices so that the rise time is equal to the double-support duration. In this way, the tracking error in the double-support phase is reduced using a gradual variation in the GRF.

By solving the ASLIP double-support dynamic equations (14) with the same initial condition as the ATRIAS COM at the current double-support phase, control law (20) results in an ASLIP double-support trajectory in numerical simulation. Using the resultant leg forces as commands, the algorithm can calculate the leg angles and horizontal/vertical components of the GRF for each leg. These forces would be the desired leg force profiles for ATRIAS in the double-support phase.

4.2. Lower level controller

In the lower level controller, the ASLIP-generated GRF profile serves as a reference for ATRIAS. For this approach to be successful, the ATRIAS and ASLIP model must be similar enough; thus, we assume that ATRIAS has virtual legs from its COM to its toes. The lower level control includes stance leg control, swing-leg control, and torso-angle control. The stance leg feedback loop uses force control, the swing leg loop uses position control along a desired path, and the torso loop has a force-angle-deviation controller.

4.2.1. Stance leg control. To control the stance leg of ATRIAS, its motors are commanded to track ASLIP toe force profiles generated in the upper level control using laws (17) and (20) for each of the walking phases. The algorithm converts the toe forces into motor torques by the mapping in (8). Then we choose a PID force control for the stance leg motors similar to that used in the stance phase of running from[17]

$$u_i = \frac{K_s}{K_g}\Delta\theta_i^s + K_P\left(\frac{T_i^{s,d}}{K_s} - \Delta\theta_i^s\right) + K_I\int\left(\frac{T_i^{s,d}}{K_s} - \Delta\theta_i^s\right)dt + K_D\left(\frac{\dot{T}_i^{s,d}}{K_s} - \Delta\dot{\theta}_i^s\right) \tag{21}$$

in which u_i is the torque of motor i of a stance leg, $\Delta\Theta_i^s$ is the deflection of the torsional spring i, and $T_i^{s,d}$ is the desired torque of spring i. In this controller, the proportional and derivative parts control the value and time rate of the toe force, whereas the integral part controls the applied ***impulse*** to the robot. Since the momentum of a system varies with the applied impulse, controlling the applied impulse (to a system with known initial velocity) will determine its final velocity at the end of the phase.

4.2.2. Swing leg control. In the single-support phase, in order to ensure smooth movement of leg 2 from takeoff to touchdown we define a parabolic curve for point E (toe of swing leg) as (22).

https://doi.org/10.1017/S0263574719001553 Published online by Cambridge University Press

The coefficients are calculated using the position of the swing toe and the hip joint at the beginning and end of single-support phase, taken from the SLIP gait.

$$y_{E_d} = c_1 x_{E_d}^2 + c_2 x_{E_d} + c_3 \tag{22}$$

After establishing y_{E_d} as a function of x_{E_d}, the algorithm needs to plan a time trajectory for x_{E_d} for which we examine two trajectory types:

1. As the first solution, constant velocity is assumed for $x_{E_d}(t)$ during the time duration t' of the SLIP single-support phase over the distance of SLIP swing toe range on the ground.
2. The second solution for trajectory profile $x_{E_d}(t)$ starts with velocity zero, accelerates with constant acceleration a' up to time $t'/2$, and then decelerates with constant acceleration $-a'$ to end with velocity zero at time t' to reach the touchdown point of SLIP model.

Using the real position of the hip joint and the desired toe position at each instance, the algorithm calculates the desired angle of the leg links. A PID controls the position of the swing leg in order to track its desired trajectory

$$u_i = K_P \left(q_{i+2}^d - q_{i+2}\right) + K_I \int \left(q_{i+2}^d - q_{i+2}\right) dt + K_D \left(\dot{q}_{i+2}^d - \dot{q}_{i+2}\right) \tag{23}$$

in which u_i is the torque of motor i of the swing leg and q_{i+2} is its relevant harmonic drive output angle (Fig. 1). Because of different loads, different PID coefficients are needed for the stance leg and swing leg. A numerical optimization problem minimizes position error of ATRIAS swing toe at touchdown x_E^{TD} for one step of a typical walking gait (Figs. 2 and 4), where the optimization parameters are PID coefficients.

$$\min_{K_P, K_I, K_D} \left| x_E^{TD} - x_A - a_{\text{SLIP}} \right| \tag{24}$$

4.2.3. Torso angle control. The body mass model signifies the major difference between the ATRIAS and SLIP models. The body mass of SLIP is a point mass on the hip, whereas the torso of ATRIAS is a distributed mass with a moment of inertia. Therefore, in addition to control of ATRIAS COM based on SLIP model, its torso angle should be controlled independently. To this purpose, we use a PD controller that deviates the desired angle of GRF with the amount of $\delta\theta_{\text{GRF}}$ to return the torso angle to zero.

$$\delta\theta_{\text{GRF}} = K_p^F \left(q_{ss_9}\right) + K_d^F \left(\dot{q}_{ss_9}\right) \tag{25}$$

In the above equation, K_p^F and K_d^F are proportional and differential coefficients of force angle controller, and q_{ss_9} is the ATRIAS torso angle. This controller generates a torque around the COM of ATRIAS, and rotates its torso in the opposite direction of the torso angle.

4.3. Overall two-level controller

Figure 6 shows the schematic block diagram of the proposed two-level controller as well as output parameters for each controller. The relevant equation number is written inside each block for easy reference.

5. Results

5.1. Numerical parameters

The kinematic and kinetic models in our ATRIAS simulation use the real robot's parameters.[17] Regarding ATRIAS parameters, its equivalent SLIP model has a free leg length of $l_0 = 0.95$ m, spring stiffness of $K_{\text{SLIP}} = 16,000$ N m, and point mass $m = 61.90$ kg equal to ATRIAS total mass. A periodic SLIP walking gait with forward velocity of $V_x = 1.15$ m/s defines the desired gait. The optimization procedure (16) using constrained Newtonian optimization of MATLAB fmincon produces initial conditions $\theta_{TD} = 21.15°$ and $\mathbf{x}_{\text{ss},0}^{\text{SLIP}} = [0.9478 \quad 0.1939 \quad 0.001584 \quad -1.2408]^T$ for the periodic gait.

https://doi.org/10.1017/S0263574719001553 Published online by Cambridge University Press

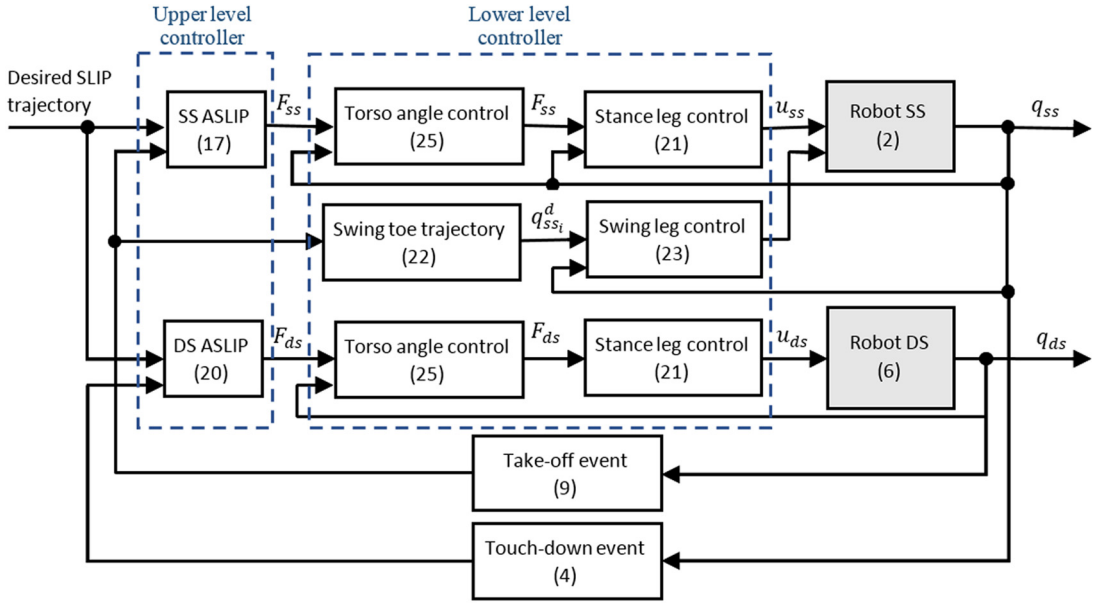

Fig. 6. The proposed two-level controller scheme.

In the upper level control (17), a value of the coefficient is selected manually as $K_p^E = 120$ so that the tracking error approaches gently to zero during the single-support phase without generating large variations in leg force.

In the lower level control for stance leg control (21), the PID coefficients for proper force tracking have been selected manually as $K_P = 5000,\ K_I = 10,000,\ K_D = 50$. Due to possible saturation of the ATRIAS motors, we put a ± 13 N m saturation block to the output of control law. To ensure the swing toe clears the ground, we assume its height in mid-stance in (22) as $y_{E_{mid}} = 0.06$ m. For swing leg control (23), PID coefficients resulted by Newtonian optimization (24) using fmincon have the values of $K_P = 1033,\ K_I = -66.2,\ K_D = 69.5$. The controller coefficients values in (25) to minimize torso angle error at the end of single-support phase are $K_p^F = 0.6,\ K_d^F = 0.3$ using a search algorithm.

5.2. Simulation results

In the results section, we refer to the upper level numerical procedure that generates the GRF profiles, that is, the SLIP-plus-feedback-control simulation, as the *virtual simulation* since this numerical procedure would be required even when controlling a real robot. The simulation of ATRIAS is referred to as the *experimental simulation,* as this would be replaced by the experimental ATRIAS robot.

Initializing consists of finding a condition for the desired periodic walking gait of SLIP model (Fig. 5) and then calculating the state vector for ATRIAS in the single-support phase (using numerical rooting to generate the same COM state vector for ATRIAS as with SLIP in its initial condition). In this procedure, we assume the deflection of the torsional springs of the takeoff leg is zero and the angular velocity of both sides are equal. In order to show robustness to uncertainty in the initial conditions, we perturb the initial stance state vector of ATRIAS by a uniformly distributed pseudorandom vector with $\pm 10\%$ amplitude and apply it to all simulations with accelerated and decelerated toe.

In the upper level, the ASLIP virtual simulation rejects disturbances and follows the SLIP gait very well in both walking phases.

In the single-support phase, ASLIP has 2 DOF and only one control input (for energy level). Figure 7 shows the energy-level tracking error of ASLIP in the single-support phase (virtual simulation). Figure 7(a) corresponds to three steps of walking with constant velocity of x_{E_d} having no deviated initial condition. Figure 7(b) is for four steps of walking with accelerated swing x_{E_d} having $\pm 10\%$ uniformly distributed deviations of initial condition. The planned swing toe error in each step starts with a nonzero value and approaches zero during the single-support phase.

For the double-support phase, Fig. 8 shows the result of the virtual ASLIP simulation with control law (20). In this phase, the 2 DOF of ASLIP are fully actuated and controllable. The tracking error

https://doi.org/10.1017/S0263574719001553 Published online by Cambridge University Press

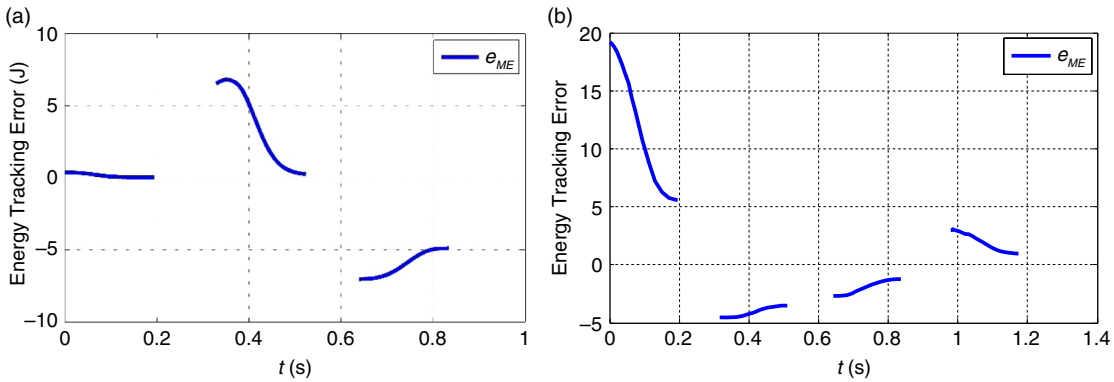

Fig. 7. Energy-level tracking error of ASLIP in single-support phase (a) for three steps of ATRIAS unstable walking with constant velocity of x_E (b) for four steps of ATRIAS stable walking with accelerated and decelerated x_E.

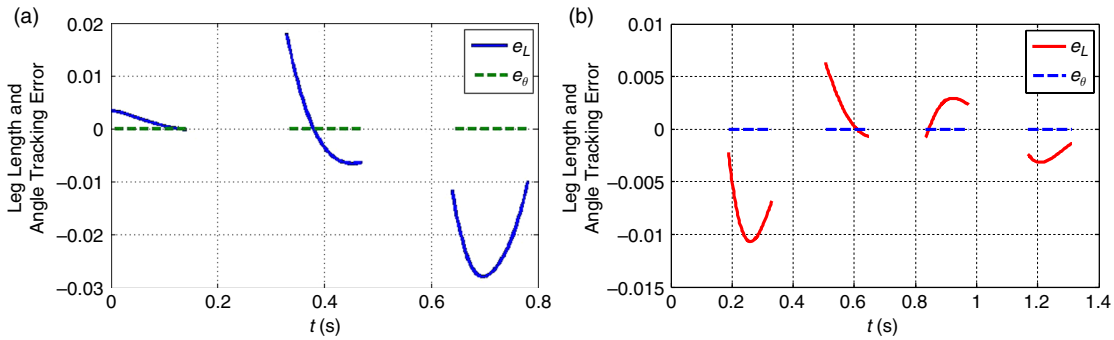

Fig. 8. Trajectory tracking error of ASLIP in double-support phase (a) for three steps of ATRIAS unstable walking with constant velocity of x_E (b) for four steps of ATRIAS stable walking with accelerated and decelerated x_E.

components include leg length error (shown by thick blue curves) and leg angle error (shown by thin green line with zero value). One conventional method of trajectory tracking in fully actuated systems is to determine coordinates $\mathbf{q}^{\mathrm{SLIP}}$ desired trajectory as a function of time and to calculate the error vector using the current coordinates $\mathbf{q}^{\mathrm{ASLIP}}$ in each instance. However, this method would cause instability of the controller for the case when the ASLIP leg angle is larger than the SLIP leg angle at the beginning of the stance phase. In these cases, instead of forward motion, the controller tries to move ASLIP backwards in order to match SLIP trajectory. This action generates improper GRFs in double-support phase and sometimes the foot takes off early in the double-support phase. Thus, instead of interpolating the desired SLIP state vector with a time index we interpolate it using the leg angle q_2'. The error vector then follows from the desired state vector of ASLIP at the current leg angle. In the virtual simulation, the leg angle error remains zero and the leg length error is converging toward zero (Fig. 8).

In the experimental simulation that includes the lower level control, ATRIAS tracks the planned toe force profiles of ASLIP. Figure 9 shows the desired and real GRF components for one leg of ATRIAS. Figure 9(a) depicts three walking steps with a fixed value of horizontal velocity of the swing toe that becomes unstable, and Fig. 9(b) shows four steps of walking with an accelerated and decelerated toe that is stable. In Fig. 9(b), the time interval from 0 to 0.19 s is related to leg 1 of the single-support phase, and the time interval 0.19–0.33 s is for leg 1 of the double-support phase. At the end of this interval, one step of walking has been completed and the leg numbers become switched for the next step. The time interval 0.33–0.52 s is related to leg 2 of the single-support phase, the swing leg, and thus no GRF exists. The curves in time interval 0.52–0.67 s represent the GRF components of leg 2 in the double-support phase. At the end of this interval, the two walking gaits of the robot and one periodic orbit for one leg of the robot has been completed. In Fig. 9, the solid cyan lines depict ASLIP GRF profiles from the SLIP gait using control laws (17) and (20);

https://doi.org/10.1017/S0263574719001553 Published online by Cambridge University Press

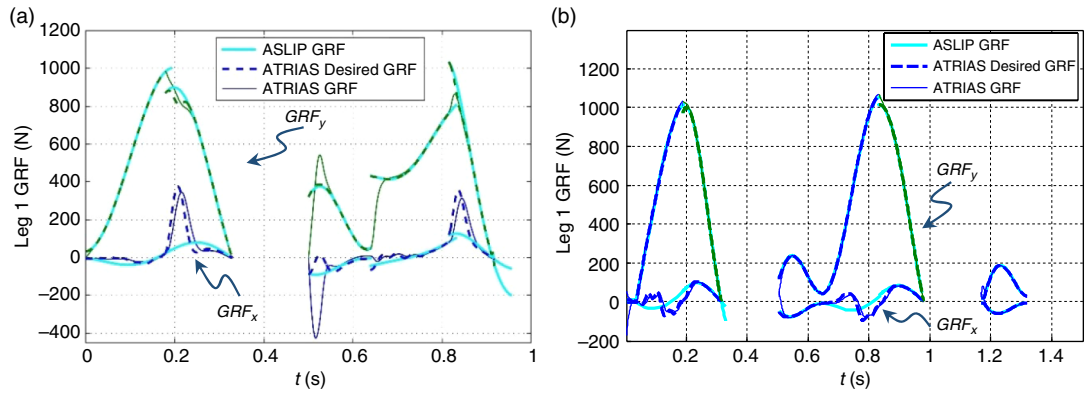

Fig. 9. Vertical and horizontal components of the desired and real GRFs for one leg of ATRIAS (a) for three steps of ATRIAS walking with constant velocity of x_E (b) for four steps of ATRIAS walking with accelerated and decelerated x_E.

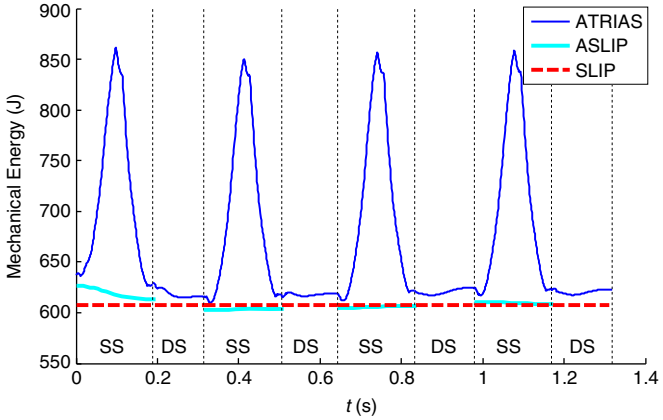

Fig. 10. Mechanical energy of SLIP, ASLIP, and ATRIAS for four steps of ATRIAS walking.

dashed lines represent ATRIAS's desired GRFs in order to keep the torso upright using control law (25). Oscillations and deviations of the desired force profile from the ASLIP force profile are due to the attempts to keep torso equilibrium. Thin (blue and green) solid lines depict ATRIAS's resulting GRFs generated by control law (21) and the ATRIAS dynamic model solved during walking phases. Blue curves having both positive and negative small values show horizontal components and green curves (with only positive values) show the vertical components of GRFs. At the beginning of each step there is a deviation from the initial condition of the nominal SLIP gait, and so the generated desired force profiles for ATRIAS by ASLIP in each step have deviations from the nominal SLIP gait. The deviation in initial condition at each step is due to the existence of force tracking errors, trajectory tracking errors, and the imprecise touchdown state due to having series springs with motors and damping in the system (although series spring have the advantage of isolating motors from touchdown impact, they generate undesirable vibrations in the swing leg and cause errors in trajectory tracking and touchdown).

The variations in mechanical energy of ATRIAS, single-support ASLIP, and SLIP model for four steps of stable walking with $\pm 10\%$ deviated initial condition are depicted in Fig. 10. The acronyms SS and DS specify single-support and double-support phase, respectively. Note that the ASLIP energy level approaches the SLIP energy level in two initial steps, and still remains in the vicinity for the subsequent steps. However, the ATRIAS mechanical energy is larger and has considerably larger variations due to the rotational energies of its rigid body parts.

The ATRIAS motor torques for five steps of walking with accelerated velocity of x_E are shown in Fig. 11. Solid lines stand for the single-support phase and dashed lines for the double-support phase. The torques of motors 1, 2, 3, and 4 are shown by lines with thicknesses 1, 2, 3, and 4, respectively. The saturation torques of the motors in ATRIAS are 13 N m. Due to the short interval of single-support phase and undesirable passive vibrations of leg links, the swing leg needs to reach the

https://doi.org/10.1017/S0263574719001553 Published online by Cambridge University Press

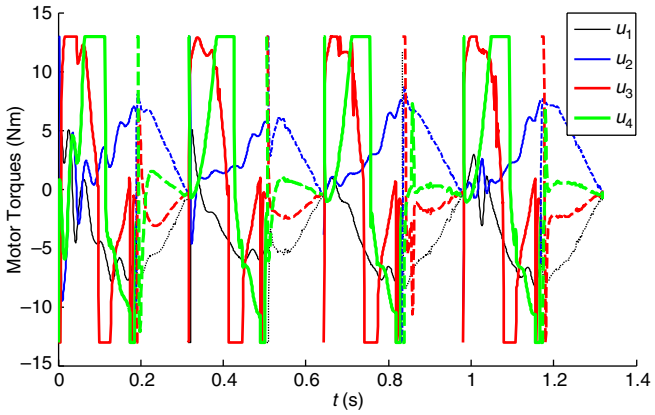

Fig. 11. ATRIAS motor torques for four steps of SLIP-based walking with accelerated velocity of x_E.

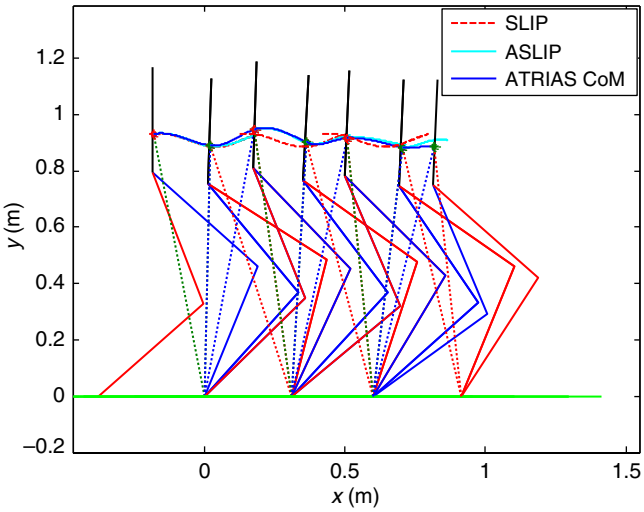

Fig. 12. Stick diagram of three steps of SLIP-based walking of ATRIAS with constant velocity of x_E.

desired touchdown length and angle in almost the minimum possible time. This effort causes torque saturation of the swing leg motors in stance phase. If the settling time of the ASLIP controllers (17) and (20) are chosen very small, then ASLIP converges to the SLIP trajectory quickly but ATRIAS motors cannot track the resulting signals and the gait becomes unstable. To avoid this problem, we choose the rise time of the ASLIP controllers for each walking phase almost equal to time interval of that phase.

The stick diagram for three steps of unstable walking using the designed two-level controller with a fixed velocity of x_E is shown in Fig. 12, and four primary steps of stable walking with accelerated and decelerated x_E appear in Fig. 13. In these figures there are three COM trajectories including the SLIP trajectory, the ASLIP trajectory, and the ATRIAS COM trajectory. The trajectory of the desired SLIP gait has been plotted by a dashed red line. Cyan thick curves depict the ASLIP trajectory that jumps to ATRIAS COM position at the beginning of each walking phase and then tracks SLIP energy level and trajectory using control laws (17) and (20). Blue thin curves are the ATRIAS COM trajectory resulting from tracking the ASLIP toe force profiles using (21). Trajectory errors increase at each step using the controller with a fixed horizontal velocity of swing leg and the robot with no deviated initial condition falls down in fourth step (Fig. 12). For the controller with accelerated swing leg, the errors are reduced and restricted to a limited bound – generating a stable walking motion even with $\pm 10\%$ deviated initial condition (Fig. 13).

Each step of ATRIAS starts with initial condition errors due to the system underactuation, touchdown impact, existence of series elastic actuation system, and tracking errors of the controllers. Also, there are some tracking errors between ASLIP and SLIP models that are due to ASLIP underactuation

https://doi.org/10.1017/S0263574719001553 Published online by Cambridge University Press

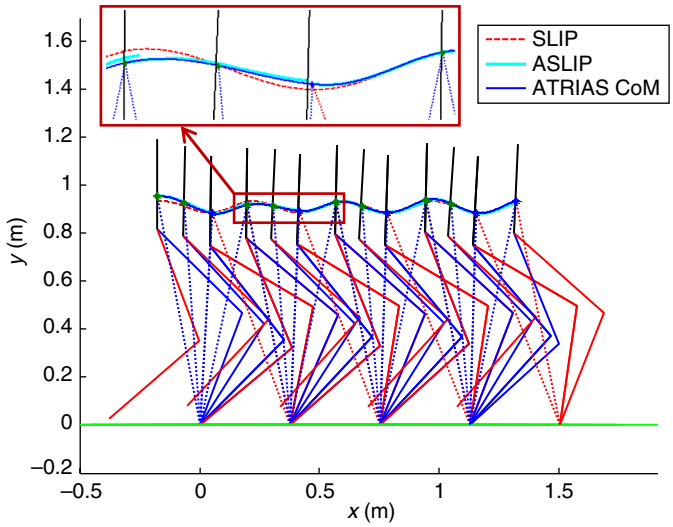

Fig. 13. Stick diagram of four steps of SLIP-based walking of ATRIAS with accelerated velocity of x_E.

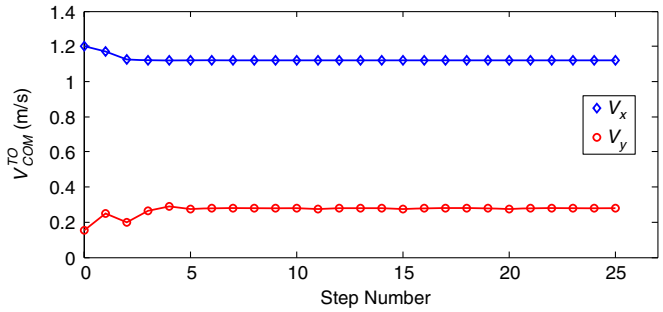

Fig. 14. Post touchdown horizontal and vertical components of ATRIAS COM velocity for 25 steps of SLIP-based walking with accelerated velocity of x_E.

in single-support phase and choosing not very large coefficients of the feedback linearization controller because of the mentioned considerations in double-support phase. Small deviations between ATRIAS COM and ASLIP trajectories are due to toe force tracking errors resulted mainly from motors saturation. The force tracking errors are maintained small enough by PID controller to be compensated at the next step and generate a stable and steady walking motion. Note that for this robot the touchdown event causes very low energy loss (about %0.1) mainly due to three qualities: the series-elastic actuation, relatively low velocities during walking, and very light-weight legs compared to the torso mass.

To show stability and steadiness of the generated walking motion, horizontal and vertical components of the ATRIAS COM velocity just after touchdown for 25 steps of walking with accelerated and decelerated x_E and $\pm 10\%$ deviated initial condition is demonstrated in Fig. 14. It shows that the COM velocity fluctuates considerably during initial four steps, then converges to a very narrow range around 1.2 m/s and remains steadily in that range. Its oscillations for walking with unlocked torso is much less than for running,[17] because walking has less degrees of underactuation than running. According to Fig. 14 the horizontal velocity of the robot COM (forward velocity) converges to a value 2.6% less than the desired value for SLIP gait. This velocity deviation is inevitable in this control strategy because of complicated multibody hybrid dynamics, damping, the unlocked torso of the robot, and the system underactuation.

5.3. Real-time execution considerations

Our simulations show that the proposed controller in this paper is implementable in real time. The most time consuming calculations are related to solving differential equations for ASLIP GRF

https://doi.org/10.1017/S0263574719001553 Published online by Cambridge University Press

planning in upper level control. In single-support phase, the numerical solution of differential equation (12) with control law (17) has an average time step of 7.6 ms. The average execution time for each time step with its GRF calculations is 11.9 ms using MATLAB on a computer with 3.5 GHz processor. Moreover, its equivalent C code takes just 0.24 ms for each time step, appropriate for real-time implementation. This is the main advantage of using SLIP in the higher level control, since equivalent numerical optimization and simulation with the ATRIAS model would most likely not run in real time with current technology.

6. Conclusions

In this work we designed and implemented a two-level control strategy for stable biped walking, suitable for the experimental biped robot known as ATRIAS. Since the ATRIAS dynamics are complex, in our novel approach ATRIAS follows some simple calculated SLIP dynamics, that is, SLIP motion defines a template, while ATRIAS is the anchor. To prevent instability of the template, we developed active SLIP models for each walking phase. In this upper level control, we choose the ASLIP controller gains such that the rise time is almost equal to the relevant phase duration. The trajectory of ASLIP is kept in a vicinity of the SLIP model, which avoids error accumulation. These high-level controls run in an ASLIP simulation, the virtual simulation, that results in a reference GRF profile (which the low-level ATRIAS controls can track). Because the ATRIAS torso is free to rotate (unlike SLIP), the low-level controls must also regulate torso angle. In addition, we also show that planning an appropriate trajectory and velocity profile for the swing leg has a vital role in gait stability. We find that a constant horizontal velocity for swing toe generates motors torques saturation, high tracking errors, and gait instability. Therefore, we tried planning acceleration and deceleration profiles for the swing toe, with zero velocity at takeoff and touchdown, and found this results in a stable gait. Simulations of the ATRIAS dynamics with control, the experimental simulations, show that the proposed control generates a steady and stable walking gait with up to $\pm 10\%$ uniformly distributed deviated initial condition. For some uniformly distributed deviations with larger amplitude, the walking motion becomes unstable. This controller results in improved computationally efficiency compared to other methods, for example, hybrid zero dynamics, and provides a framework for control of underactuated robots. Due to our use of a leg force controller, this controller has the potential for improved walking and running on uneven and soft terrains.

For future work, this control strategy can guide the real robot walking and running, allowing determination of robustness to terrain softness. Also, SLIP could be replaced by an active template model, like point mass biped (PMB),[26] which should be able to generate more general gaits including asymmetric trajectories.

Acknowledgements

This work was supported by the Office of Research Affairs at the University of Tabriz for the research project s/27/3570-6.

References

1. M. Vukobratovic, D. Stokic, B. Borovac and D. Surla, *Bipedal Locomotion* (Springer-Verlag, Berlin, Heidelberg, 1990). doi:10.1007/978-3-642-83006-8_1
2. P. Piiroinen and H. Dankowicz, "Low-cost control of repetitive gait in passive bipedal walkers," *Int. J. Bifurcat. Chaos* **15**(6), 1959–1973 (2005).
3. Y. Hurmuzlu, "Dynamics of bipedal gait; Part I – objective functions and the contact event of a planar five link biped, Part II – stability analysis of a planar five link biped," *ASME J. Appl. Mech.* **60**(2), 331–344 (1993).
4. J. W. Grizzle, G. Abba and F. Plestan, "Asymptotically stable walking for biped robots: Analysis via systems with impulse effects," *IEEE Trans. Automat. Contr.* **46**(1), 51–64 (2001).
5. C. Chevallereau, E. R. Westervelt and J. W. Grizzle, "Asymptotically stable running for a five-link four-actuator planar bipedal robot," *Int. J. Robot. Res.* **24**(6), 431–464 (2005).
6. Y. Hu, G. Yan and Z. Lin, "Stable running of a planar underactuated biped robot," *Robotica* **29**(5), 657–665 (2011).
7. B. Dadashzadeh, M. J. Mahjoob, M. Nikkhah Bahrami and C. Macnab, "Stable active running of a planar biped robot using Poincare map control," *Adv. Robot.* **28**(4), 231–244 (2014).
8. R. Blickhan, "The spring-mass model for running and hopping," *J. Biomech.* **22**(11–12), 1217–1227 (1989).
9. H. Geyer, A. Seyfarth and R. Blickhan, "Compliant leg behavior explains basic dynamics of walking and running," *Proc. Royal. Soc. B* **273**, 2861–2867 (2006).

10. J. Schmitt and J. Clark, "Modeling posture-dependent leg actuation in sagittal plane locomotion," *Bioinsp. Biomim.* **4**(4), 046005 (2009).
11. A. Seyfarth, H. Geyer and H. Herr, "Swing-leg retraction: A simple control model for stable running," *J. Exp. Biol.* **206**, 2547–2555 (2003).
12. J. Englsberger, P. Kozlowski and C. Ott, "Biologically Inspired Dead-Beat Controller for Bipedal Running in 3D," *2015 IEEE/RSJ International Conference on Intelligent Robots and Systems (IROS)*, Hamburg, Germany (2015) pp. 989–996.
13. Z. Xu and J. Gao, "Robot simulations based on bipedal spring-mass model with variable slack length and stiffness," *IEEE Access* **5**, 2169–3536 (2017).
14. S. H. Tamaddoni, F. Jafari, A. Meghdari, and S. Sohrabpour, "Biped hopping control based on spring loaded inverted pendulum," *Int. J. Hum. Robot.* **7**(2), 263–280 (2010).
15. I. Poulakakis and J. W. Grizzle, "The spring loaded inverted pendulum as the hybrid zero dynamics of an asymmetric hopper," *IEEE Trans. Automat. Contr.* **54**(8), 1779–1793 (2009).
16. G. Garofalo, C. Ott and A. Albu-Schaffer, "Walking Control of Fully Actuated Robots Based on the Bipedal SLIP Model," *IEEE International Conference on Robotics and Automation*, St Paul, MN, USA (2012).
17. B. Dadashzadeh, H. R. Vejdani and J. Hurst, "From Template to Anchor: A Novel Control Strategy for Spring-Mass Running of Bipedal Robots," *IEEE/RSJ International Conference on Intelligent Robots and Systems (IROS 2014)*, Chicago, IL, USA (2014) pp. 2566–2571.
18. A. Hereid, S. Kolathaya, M. S. Jones, J. Van Why, J. W. Hurst and A. D. Ames, "Dynamic Multi-Domain Bipedal Walking with ATRIAS Through SLIP based Human-Inspired Control," *Proceedings of the 17th International Conference on Hybrid Systems: Computation and Control (HSCC'14)*, New York, NY, USA (2014) pp. 263–272.
19. A. Ramezani, J. Hurst, K. Akbari Hamed and J. W. Grizzle, "Performance analysis and feedback control of ATRIAS, a three-dimensional bipedal robot," *J. Dyn. Syst. Meas. Contr.* **136**(2) (2013). doi:10.1115/1.4025693.
20. S. Rezazadeh and J. W. Hurst, "Toward Step-by-Step Synthesis of Stable Gaits for Underactuated Compliant Legged Robots," *IEEE International Conference on Robotics and Automation (ICRA)*, Seattle, WA, USA (2015) pp. 4532–4538, ISSN 1050-4729.
21. G. Gupta and A. Dutta, "Trajectory generation and step planning of a 12 DoF biped robot on uneven surface," *Robotica* **36**(7), 945–970 (2018).
22. V. Janardhan and R. Prasanth Kumar, "Generating real-time trajectories for a planar biped robot crossing a wide ditch with landing uncertainties," *Robotica* **37**(1), 109–140 (2019).
23. S. Kajita, M. Benallegue, R. Cisneros, T. Sakaguchi, S. I. Nakaoka, M. Morisawa, H. Kaminaga, I. Kumagai, K. Kaneko and F. Kanehiro, "Biped Gait Control Based on Spatially Quantized Dynamics," *IEEE-RAS 18th International Conference on Humanoid Robots (Humanoids)*, Beijing, China (2018) pp. 75–81.
24. C. Hubicki, J. Grimes, M. Jones, D. Renjewskiy, A. Sprowitzz, A. Abate and J. Hurst, "ATRIAS: Design and validation of a tether-free 3D-capable spring-mass bipedal robot," *Int. J. Robot. Res.* **35**(12), 1497–1521 (2016).
25. B. Dadashzadeh and M. J. Mahjoob, "Dynamics Synchronization of the Running of Planar Biped Robots with SLIP Model in Stance Phase," *The 2nd ICRoM International Conference on Robotics and Mechatronics*, Tehran, Iran (2014).
26. B. Dadashzadeh, M. Esmaeili and C. Macnab, "Arbitrary symmetric running gait generation for an underactuated biped model," *PloS one* **12**(1), e0170122 (2017).